Materials Chemistry and Physics 143 (2014) 1026–1031

Contents lists available at ScienceDirect

Materials Chemistry and Physics

journal homepage: www.elsevier.com/locate/matchemphys

Elasticity and yield strength of pentagonal silver nanowires: In situ bending tests

Sergei Vlassov [a,b,c,*], Boris Polyakov [c], Leonid M. Dorogin [a,b], Mikk Antsov [a,b], Magnus Mets [a], Madis Umalas [a], Rando Saar [a], Rünno Lõhmus [a,b], Ilmar Kink [a,b]

[a] Institute of Physics, University of Tartu, Riia 142, 51014 Tartu, Estonia
[b] Estonian Nanotechnology Competence Centre, Riia 142, 51014 Tartu, Estonia
[c] Institute of Solid State Physics, University of Latvia, Kengaraga 8, LV-1063 Riga, Latvia

HIGHLIGHTS

- Mechanical properties of pentagonal silver nanowires were measured.
- Cantilevered beam bending technique was used.
- Measurements were performed inside a scanning electron microscope.
- Young's modulus and yield point were calculated.
- Both plastic deformation and fracture of nanowires were observed.

ARTICLE INFO

Article history:
Received 29 March 2013
Received in revised form
23 October 2013
Accepted 29 October 2013

Keywords:
Electron microscopy
Mechanical testing
Elastic properties
Fracture
Fatigue

ABSTRACT

This paper reports in situ mechanical characterization of silver nanowires (Ag NWs) inside a scanning electron microscope using a cantilevered beam bending technique. Measurements consisted in controlled bending of a cantilevered NW by the tip of an atomic force microscope glued to the force sensor. Relatively high degree of elasticity followed by either plastic deformation or fracture was observed in bending experiments. Experimental data were numerically fitted into the model based on the elastic beam theory and values of Young modulus and yield strength were extracted. Measurements were performed on twenty Ag NWs with diameters from 76 nm to 211 nm. Average Young modulus and yield strength were found to be 90 GPa and 4.8 GPa respectively. In addition, fatigue tests with several millions of cycles were performed and high fatigue resistance of Ag NWs was demonstrated.

1. Introduction

Silver nanowires (Ag NWs) are promising material for nanoscale systems due to their excellent electrical and thermal conductivity [1,2], perfect structure, and ease of synthesis. Among other applications, Ag NWs are considered as an alternative and even replacement to indium tin oxide (ITO) in making transparent, flexible, and conductive films [3–6]. Possessing the ability of localizing electromagnetic energy in regions much smaller than the wavelengths of light and being the metal with the lowest losses in the visible spectrum [7], Ag NWs can also serve as waveguides for plasmon propagation in nanophotonics [8]. Besides the electrical and optical properties, mechanical characteristics are also of a great importance for performance of the named systems. In many applications NWs are subjected to mechanical stresses and deformations. In flexible electrodes, as well as in various nanoelectromechanical systems (NEMS) like e.g. nanorelays, nanoswitches [9] and nanoresonators [10], NWs should withstand numerous repetitive deformations. In nanophotonics large degree of bending deformation of NW is often required to guide the light in desired direction. It was also shown that defects or discontinuities such as cracks introduced by bending of Ag NW strongly affect surface plasmon resonance and light propagation in waveguides [8,11]. Therefore a deeper understanding of elasticity, plasticity, fatigue and fracture of Ag NWs is essential for performance and reliability of above mentioned devices.

* Corresponding author. Institute of Physics, University of Tartu, Riia 142, 51014 Tartu, Estonia. Tel.: +372 55 941 841.
E-mail address: vlassovs@ut.ee (S. Vlassov).

0254-0584/$ – see front matter © 2013 Elsevier B.V. All rights reserved.
http://dx.doi.org/10.1016/j.matchemphys.2013.10.042

Ag NWs among other metallic FCC NWs are known to form pentagonal crystals with remarkable properties. Fivefold symmetry in such NWs is conditioned by twin boundaries dividing five regular crystalline domains [12]. The specific structure of these NWs leads to the presence of intrinsic elastic strain that in turn promotes various mechanisms of stress relaxation [13]. Thus, a NW with the peculiar internal structure and accumulated stress-induced defects is expected to exhibit mechanical properties different from those of the regular crystallinity [14].

There were several methods employed for mechanical characterization of pentagonal Ag NWs, namely, nanoindentation, three point bending test and tensile test. Lucas et al. [15] studied plastic deformation of a pentagonal Ag NWs by nanoindentation using an atomic force microscope (AFM). Three point double-clamped beam bending tests were performed by Wu et al. [14] and Jing et al. [16]. In this method a suspended Ag NW fixed from both ends was bent in the midpoint by the tip of AFM whilst Young modulus and yield strength were calculated. Zhu et al. performed *in situ* tensile tests of Ag NWs inside a scanning electron microscope (SEM) [17]. NW was fixed between the nanomanipulator tip and AFM cantilever and then pulled until failure. Young's modulus, yield strength, and ultimate strength were calculated from the deflection of the AFM cantilever with known spring constant. Young modulus and yield strength of Ag NWs measured by all listed methods were typically higher than for bulk silver. Dependence of mechanical properties on size was reported for diameters smaller than 100 nm [16,17]. Moreover, limited plasticity of Ag NWs during fracture was reported both by Wu and Zhu [14,17]. It should be noted, that nontrivial fracturing behavior was observed also for some other metallic NWs. For example Peng et al. found a size dependent fracture mode for Cu NWs in tensile tests, demonstrating that with decreasing diameter NWs behave more brittle [18]. Wang et al. investigated strength of thin Au NWs by *in situ* tensile tests inside TEM and found complicated fracturing scenarios of NWs exhibiting ductile-to-brittle transition depending on twin size [19]. Therefore, deformation and fracture mechanics of metallic NWs is an intriguing topic deserving a particular attention.

Moduli and strengths of crystalline anisotropic materials depend on test conditions. Therefore, although above mentioned methods cover a wide range of mechanical properties, results cannot be extended to all types of deformation. In many important applications, like already mentioned NEMS and nanoplasmonics, the pure bending takes place. To the best of our knowledge, pure bending tests of Ag NWs were not reported in literature yet. Therefore additional study of Ag NW deformation is required.

Pure bending condition is realized in a method known as cantilevered beam bending technique, that has been successfully applied for characterization of some NWs and nanotubes [20]. In this method, generally based on the AFM technique, free end of suspended NW is pushed by the AFM tip and Young modulus is calculated from the deflection of the cantilever. Main disadvantage of this method, as well as AFM based characterization in general, is lack of visual feedback during measurements, i.e. imaging is made only before and after the bending experiment. As a consequence, essential data on the NW behavior during bending like e.g. neck formation or crack propagation, are missing.

In this paper we describe application of advanced in situ cantilevered beam-bending technique [21] to measure mechanical properties and monitor deformation of Ag NWs. In contrast to traditional AFM bending tests, our measurements are performed inside SEM enabling real-time visualization of NW behavior during the measurements, and fine control over the experiment. Self-made force sensor, based on a quartz tuning fork (QTF), is used for precise data acquisition.

2. Materials and methods

2.1. Materials

Ag NWs were purchased from *Blue Nano* and had diameters in the range from tens to a few hundreds nm with average diameter of 120 nm. High resolution SEM (Helios NanoLab, FEI) images revealed straight and uniform NWs with well-pronounced pentagonal cross-section (Fig. 1).

A silicon calibration grating (TGX series, Mikromasch) was used as a substrate. The grating comprised of 1 μm deep square holes with 3 μm pitch having sharp undercut edges formed by the (110) crystallographic planes of silicon. Ag NWs were deposited on the grating from ethanol solution so that some NWs were partly suspended over the trenches.

2.2. Experimental set-up

Recently developed in situ nanomanipulation and measurement set-up [22] was used in the experiments. The system comprises of 3D nanomanipulator (SLC-1720-S, SmarAct) equipped with a self-made force sensor and installed inside a SEM (Vega-II SBU, TESCAN; typical chamber vacuum 3×10^{-4} mbar). The force sensor is made by gluing an AFM cantilever with a sharp tip (Nanosensor ATEC-CONT cantilevers $C = 0.2$ N m^{-1}) to one prong of a commercially available quartz tuning fork (QTF). The tip of ATEC-CONT cantilevers is tilted about 15° relative to the cantilever, providing the tip visibility from the top. In experiments QTF is driven electrically on its resonance frequency in self-oscillation mode. Oscillation parameters of such system strongly depend on the load acting on the tip, which enables to measure the forces involved in manipulations. The signal from the QTF was amplified by lock-in amplifier (SR830, Stanford Research Systems) and recorded through the ADC-DAC card (NI PCI-6036E, National Instruments). Typical values of the driving voltage were 20–50 mV and corresponding tip oscillation amplitude in order of 100 nm. In experiments the tip oscillated parallel to the sample surface (shear mode) and normal to NWs. The force sensitivity of the sensor was calibrated on precalibrated AFM cantilevers (FCL, AppNano and

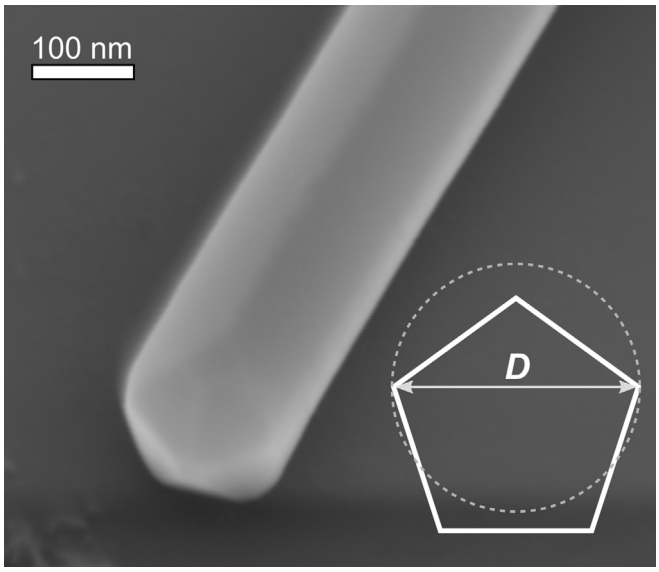

Fig. 1. SEM micrograph of one of the Ag NWs used in bending tests and schematic of pentagonal cross section with apparent diameter D. Circular cross-section of the same D is given for representative purpose.

CSG11 $C = 0.03–0.1$ N m^{-1}, NT-MDT) similar to the procedures described in Refs. [23,24]. The tip was electrically connected to the QTF electrode to exclude charging effects. To make the QTF response faster, the Q-factor was reasonably decreased by putting a small drop of epoxy resin (Ecobond 286, Emerson & Cuming) onto the opposite prong of the QTF. Schematics and actual micrographs of experimental set-up are given in supplementary data (Fig. S1 and S2).

2.3. Bending test

Advanced cantilevered beam bending scheme was employed to measure Young modulus, yield strength and fatigue of Ag NWs. Measurements consisted in visually controllable in-plane bending of half-suspended NW by the AFM tip inside the SEM with simultaneous force registration. No special procedures were needed for fastening the NWs to the substrate – the static friction between the NW and the substrate was high enough to keep the adhered part of the NW in place during the bending.

After the bending tests all NWs were characterized inside the high resolution SEM to obtain precise data on diameters and analyze the deformed area.

Numerical analysis of the bending test was based on the elastic beam theory [25] described in more details in our previous works [26]. The model enables to find out the flexural rigidity of the NW, which is a product of the Young modulus E and area moment of inertia I. Young modulus is an intrinsic property of material, and the area moment of inertia is determined by the cross-sectional geometry of the NW. Ag NW was modeled as a prismatic beam with pentagonal cross-section. Force-displacement curve within the approximation of the pure in-plane bending of an elastic beam of a given EI was calculated. Experimental and modeled force–displacement curves were fitted for the determination of E as unknown parameter. The yield point was identified as the point where curves diverge. If the tip slid along the NW during bending it was accounted in fitting procedure as the change of the beam effective length.

3. Results and discussion

Measurements were performed on twenty NWs with diameters ranging from 76 nm to 211 nm. Typically two regions were clearly distinguished on bending curves as shown in Fig. 2. In initial region (**a**–**b**) NW bends elastically and the force grows nearly linearly with the bending. It was also confirmed separately on several NWs that in the linear region the NW returns to the undeformed state upon removal of the external force. Then the slope of the force curve changes, which indicates the onset of the plastic yield. The following region (**b**–**c**) corresponds to the plastic deformation of the wire. At the region **c**–**d** the tip is retracted and the force decreases to zero. The same NW was then deformed more to find the critical deformation before the fracture. However, as seen from Fig. 2f even strongly bent NW has no signs of fracture, and deformation seems to be purely plastic, indicating significant difference of Ag NW behavior in pure bending conditions in comparison to "super elastic behavior followed by unexpected brittle failure" [17] and limited plasticity [14] reported in three point bending and tensile tests respectively.

Nevertheless about one third of NWs did break during the bending (Fig. 3). In this case three regions on the force curve can be distinguished. Incident elastic bending (**a**–**b**) is followed by a steep drop in the force (point **b**), which may correspond to a partial destruction of the NW and a crack formation. Region **b**–**c** may indicate the crack stabilization and the plastic deformation during further bending. Finally NW breaks (point **c**). Event of the breaking is accurately detected both from the video of the experiment and from the abrupt drop of the force close to zero after the point **c**.

Subsequent observation in the high-resolution SEM revealed rather brittle fracture of broken NWs without significant residual deformation (Fig 3). Such behavior is not what one would expect from the plastic material like silver, however, now it agrees better to the limited plasticity and brittle fracture reported in the tensile and three point bending tests respectively [14,17]. On the other hand, the broken end still remained partly attached to the rest of the NW in all the cases of fracture, which is not typical for purely brittle fracture. Moreover, very small, but nonzero force is still detectable after fracture, which may indicate the presence of a small neck connecting two parts of the NW.

For some NWs an intermediate state was observed, where cracks appeared, but were poorly pronounced (Fig. 4a). Interesting, that in some cases crack propagated to the half-depth of the NW cross-section where it was terminated, so that further plastic bending proceeded without the crack propagation (Fig. 4b, c). Possible explanation could be a dissipation of the crack energy in the core of the NW where all five crystallines are joined and form a disclination [13]. This hypothesis is enforced by the fact that amorphization is known to occur in disclination core [27]. Thus, the fracture mechanism seems to be more complex possessing attributes of both ductile and brittle fracture. Such duality may be related to pentagonal structure of Ag NWs, which leads to the presence of intrinsic elastic strain due to peculiarities of their fivefold twinned structure [12,13]. The intrinsic strain possessing elastic energy can facilitate the plastic flow processes. On the other side, the twin boundaries might decrease the mobility of defects.

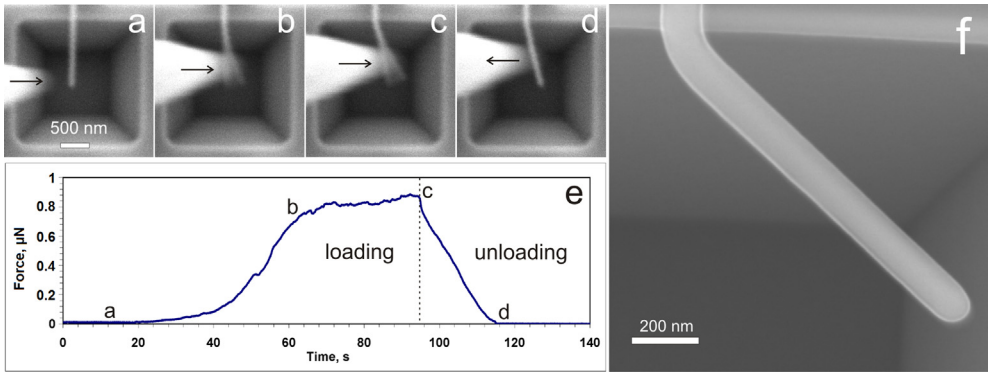

Fig. 2. Bending test of Ag NW. Selected frames from video of experiment (a–d), corresponding force curve vs. time (e), and high resolution SEM image of plastically bent NW after the experiment (f).

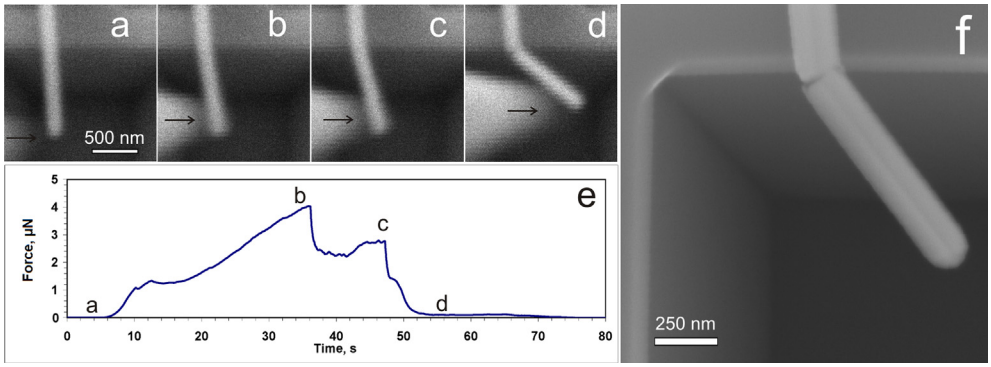

Fig. 3. Bending test of Ag NW. Selected frames from video of experiment (a–d), corresponding force curve vs. time (e), and high resolution SEM image of broken NW after the experiment (f).

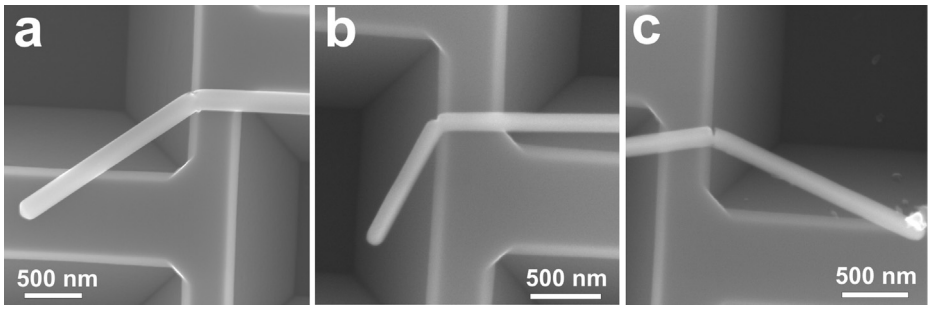

Fig. 4. Ag NWs fractured after bending. Poorly pronounced crack (a) and a crack propagated to the core of the NW.

Therefore detailed analysis and simulations of the bending deformation is required.

The degree of the deformation Ag NWs withstood prior yield and fracture was relatively high. Median curvature and strain in elastic regime were $0.8 \pm 0.3\ \mu m^{-1}$ and 0.093 ± 0.035 respectively.

Oscillation frequency of the tip in experiments was approx. 30 kHz. This allowed us to perform the fatigue tests of NWs and evaluate the influence of the tip oscillations on the NW deformation during the bending test. The tip was brought into the contact with the NW and oscillation amplitude was increased to the value close to the maximal deformation prior the plastic yield. The tip-NW system was left to oscillate for several minutes producing several millions of bending cycles. No signs of the fracture or plastic deformation, as well as changes in the force sensor signal were observed indicating a high fatigue resistance of Ag NWs. However, influence of the tip oscillation on the NW deformation during the bending tests cannot be excluded completely. For example, mechanical excitation from the QTF can lead to the heat dissipation and local elevation of the temperature. In this case an increased mobility of defects can promote the plastic regime of the deformation. Therefore problems like fatigue, as well as mechanism of deformation and fracture, need to be addressed in future researches and studied systematically. Nevertheless, it can be concluded that Ag NWs can be bent elastically multiple times to the significant curvatures without fracture and therefore are suitable for most NEMS applications.

For numerical analysis of the experimental data the force curves and NW profiles from the SEM images were fitted to the curve given by the equation of equilibrium for a bent elastic beam [26]. Fitting of the experimental and modeled force–displacement curves is shown on Fig. 5. Point of the divergence of two curves corresponds to the onset of the plastic yield.

Measured Young moduli ranged from 39 GPa to 150 GPa with the median of 90 GPa, which is only slightly higher than bulk value 83 GPa [28] of silver and is close to Young moduli obtained by other methods for similar diameters, which confirms relevance of our method (Fig. 6).

Yield strength values are scattered without pronounced peak from 1 GPa to 10 GPa with median average of 4.8 GPa. Literature data on the yield strength of Ag NWs measured in pure bending tests is absent. In tensile test for similar diameters Zhu et al. obtained yield strength of approximately 1 GPa, which is two orders of magnitude higher than the bulk value (55 MPa) [28] and approaches the theoretical strength (3.5 GPa) of Ag in the <110> direction [29]. Although for anisotropic materials the yield strength

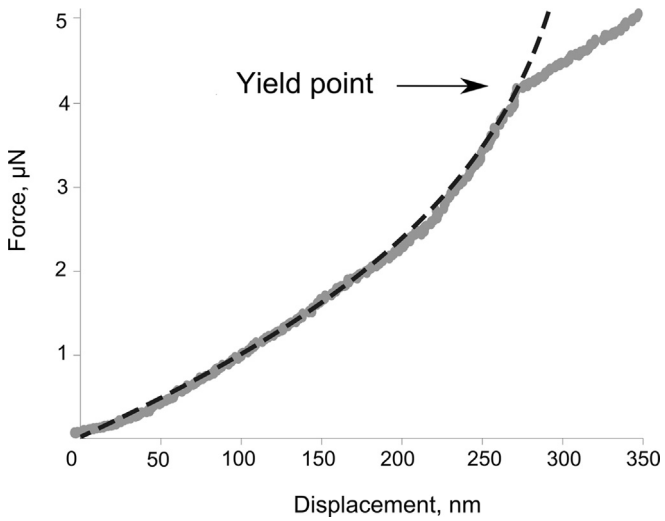

Fig. 5. Fit of the theoretical (dashed line) and experimental force–distance curves, which yields Young's modulus and yield strength of 113 GPa and 10 GPa respectively.

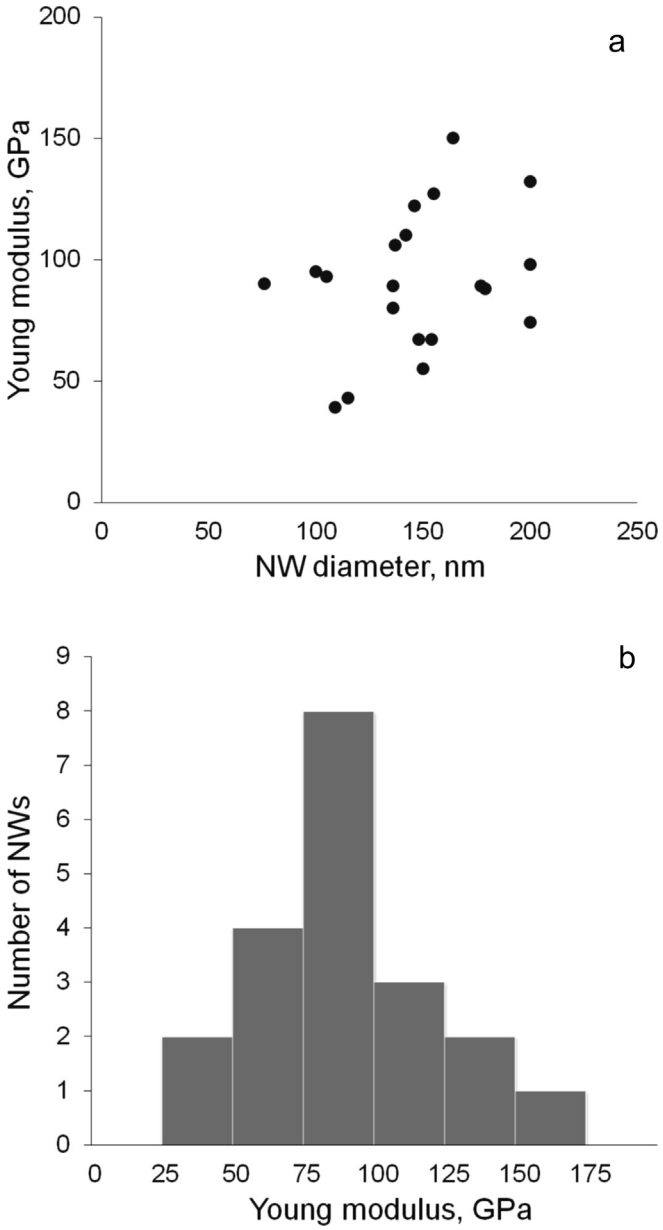

Fig. 6. Young modulus versus diameter (a) and distribution of Young moduli (b) for set of 20 NWs.

obtained by different methods cannot be compared directly, high yield strength values and broad scattering in our experiments indicate superior crystalline structure of NWs, low concentration and random distribution of defects.

Common way to represent the distribution of material's strength is Weibull statistics [30,31]. The probability of plastic deformation P_Y for a specimen at given deformation is:

$$P_Y = 1 - \exp\left[-\left(\frac{\sigma_Y}{\sigma_0}\right)^m\right], \quad (1)$$

where σ_Y is a yield strength and σ_o is the characteristic yield strength (i.e., the stress at which 63% of the specimens have failed or deformed plastically), and m is the Weibull modulus. The Weibull modulus is a dimensionless parameter of the Weibull distribution used to describe variability in the measured strength. Higher m values correspond to a steeper Weibull plot and indicate a lower dispersion of fracture stresses. In our experiment the Weibull modulus obtained for yield strength of Ag NWs was 1.31 (Fig. 7), which is lower than Zhu et al. [17] obtained in tensile test. This can be due to difference in deformation type or distribution of defects in NWs.

No correlation of measured properties with NW diameter was observed, which is in accordance to expectation for considered diameters. In other works it was shown that Young modulus approaches a constant value for Ag NWs thicker than 70 nm [16,32].

Finally we would like to discuss importance of the cross-sectional geometry of NWs within frameworks of the elastic beam theory. Although pentagonal symmetry is typical for Ag nanostructures [33,34], it is common that researchers chose circular geometry for their calculations [14,16,35]. Indeed, such assumption can be partly justified since in some cases the cross-section of Ag NWs can be considerably rounded [14]. Nevertheless, facets are still easily distinguishable, which leads to the conclusion that even in those works where rounding of cross-section takes places, the real geometry can lie somewhere between pentagon and circle.

Area moments of inertia for pentagonal I_{pent} and circular cross-section I_{circ} [36]

$$I_{pent} = \frac{1}{96}\frac{\left(3-\sqrt{5}\right)}{\left(3+\sqrt{5}\right)}\sqrt{265+118\sqrt{5}}D^4, \quad (2)$$

$$I_{circ} = \frac{\pi}{64}D^4 \quad (3)$$

where D is an apparent diameter as it is seen from the top view on a SEM image and can be understood from the inset in Fig. 1. Now if we compare Young moduli of the beams with the same D, but different cross-sections, we obtain $E_{pent}/E_{circ} = 1.405$. Thus, the circular assumption gives underestimated results in bending tests of pentagonal NWs. This can be a possible reason of low Young moduli (below bulk value) reported by some authors for Ag NWs with diameters larger than 90 nm [16].

In addition to rounding, distortions of pentagon are also reported in literature [13]. Facets, as well as the angles between the facets, are not always equal. As an example, we estimated a possible influence of unaccounted pentagon geometry distortion on Young modulus for the case of a pentagon compressed to a different extent in the direction normal to effective diameter D. For compression factor varying from 0.8 to 1.2 we obtained Young moduli of

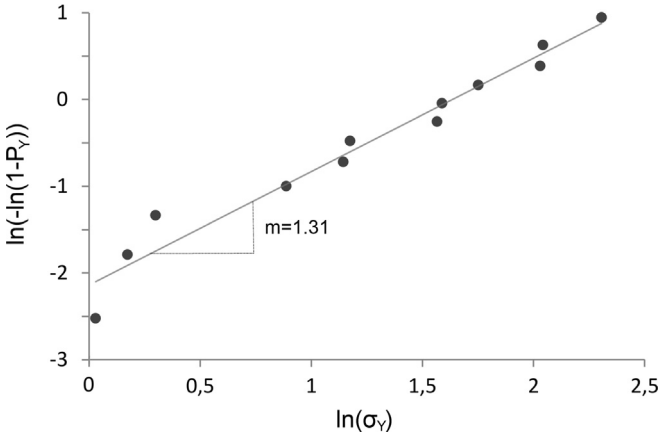

Fig. 7. Plot of Weibull statistics of yield strength for plastically deformed Ag NWs.

particular NW ranging from 115 to 75 GPa. It is necessary to note, that pentagon distortions cannot be easily detected from the top view of the SEM image if distorted facet hidden under a NW. Therefore, unaccounted deviations from regular pentagonal geometry may significantly contribute to data scattering.

4. Conclusions

Silver NWs were characterized using the cantilevered beam bending technique inside a SEM. Measurements consisted in bending of cantilevered NW by an AFM tip glued to a self-made force sensor. Under the bending load NWs demonstrated relatively high degree of elasticity followed by one of the two scenarios—plastic deformation or semi-brittle fracture. Measurements were performed on 20 Ag NWs with diameters from 76 nm to 211 nm. Median Young modulus and yield strength were found to be 90 GPa and 4.8 GPa respectively. No dependence of the mechanical properties on diameter was observed. Fatigue tests with several millions of cycles were performed and it was demonstrated that Ag NWs have high fatigue resistance and can be bent elastically multiple times to significant curvatures without failure. In addition, it was shown, that correct determination of NW cross-section geometry is crucial for calculation of its elastic properties in frames of the elastic beam theory.

Acknowledgments

This work was supported by the ESF FANAS program "Nanoparma" and EU ERDF project Centre of Excellence "Mesosystems: Theory and Applications", TK114. The work was also partly supported by the ESF project Nr. 2013/0015/1DP/1.1.1.2.0/13/APIA/VIAA/010, ETF grants 8420, 9007, Estonian Nanotechnology Competence Centre (EU29996), ERDF "TRIBOFILM"3.2.1101.12-0028, "IRGLASS" 3.2.1101.12-0027 and "Nano-Com" 3.2.1101.12-0010. We would also like to thank Professor Alexey Romanov for fruitful discussions on the structure and mechanical properties of materials with pentagonal symmetry.

Appendix A. Supplementary data

Supplementary data related to this article can be found at http://dx.doi.org/10.1016/j.matchemphys.2013.10.042.

References

[1] B. Wiley, Y. Sun, Y. Xia, Acc. Chem. Res. 40 (2007) 1067–1076.
[2] K.K. Caswell, C.M. Bender, C.J. Murphy, Nano Lett. 3 (2003) 667–669.
[3] C.–H. Liu, X. Yu, Nanoscale Res. Lett. 6 (2011) 75.
[4] P. Lee, J. Lee, H. Lee, J. Yeo, S. Hong, K.H. Nam, D. Lee, S.S. Lee, S.H. Ko, Adv. Mater. 24 (2012) 3326–3332.
[5] J. Lee, P. Lee, H. Lee, D. Lee, S.S. Lee, S.H. Ko, Nanoscale 4 (2012) 6408–6414.
[6] J.H. Lee, P. Lee, D. Lee, S.S. Lee, S.H. Ko, Cryst. Growth Des. 12 (2012) 5598–5605.
[7] P.R. West, S. Ishii, G.V. Naik, N.K. Eman, V.M. Shalaev, A. Boltasseva, Laser Photon. Rev. 4 (2010) 795–808.
[8] W. Wang, Q. Yang, F. Fan, H. Xu, Z.L. Wang, Nano Lett. 11 (2011) 1603–1608.
[9] O.Y. Loh, H.D. Espinosa, Nat. Nanotechnol. 7 (2012) 283–295.
[10] M. Li, R.B. Bhiladvala, T.J. Morrow, J.A. Sioss, K.-K. Lew, J.M. Redwing, C.D. Keating, T.S. Mayer, Nat. Nanotechnol. 3 (2008) 88–92.
[11] H.S. Park, X. Qian, J. Phys. Chem. C 114 (2010) 8741–8748.
[12] H. Chen, Y. Gao, H. Zhang, L. Liu, H. Yu, H. Tian, S. Xie, J. Li, J. Phys. Chem. B 108 (2004) 12038–12043.
[13] V.G. Gryaznov, J. Heidenreich, A.M. Kaprelov, S.A. Nepijko, A.E. Romanov, J. Urban, Cryst. Res. Technol. 34 (1999) 1091–1119.
[14] B. Wu, A. Heidelberg, J.J. Boland, J.E. Sader, X. Sun, Y. Li, Nano Lett. 6 (2006) 468–472.
[15] M. Lucas, A.M. Leach, M.T. McDowell, S.E. Hunyadi, K. Gall, C.J. Murphy, E. Riedo, Phys. Rev. B 77 (2008) 245420.
[16] G.Y. Jing, H.L. Duan, X.M. Sun, Z.S. Zhang, J. Xu, Y.D. Li, J.X. Wang, D.P. Yu, Phys. Rev. B 73 (2006) 235409.
[17] Y. Zhu, Q. Qin, F. Xu, F. Fan, Y. Ding, T. Zhang, B.J. Wiley, Z.L. Wang, Phys. Rev. B 85 (2012) 045443.
[18] C. Peng, Y. Zhan, J. Lou, Small 8 (12) (2012) 1889–1894, http://dx.doi.org/10.1002/smll.201101911.
[19] J. Wang, F. Sansoz, J. Huang, Y. Liu, S. Sun, Z. Zhang, S.X. Mao, Nat. Commun. 4 (2013) 1742, http://dx.doi.org/10.1038/ncomms2768.
[20] E.C.C.M. Silva, L. Tong, S. Yip, K.J. Van Vliet, Small 2 (2006) 239–243.
[21] B. Polyakov, L.M. Dorogin, S. Vlassov, I. Kink, A. Lõhmus, A.E. Romanov, R. Lõhmus, Solid State Commun. 151 (2011) 1244–1247.
[22] S. Vlassov, B. Polyakov, L.M. Dorogin, A. Lõhmus, A.E. Romanov, I. Kink, E. Gnecco, R. Lõhmus, Solid State Commun. 151 (2011) 688–692.
[23] S.C. Fain, K.A. Barry, M.G. Bush, B. Pittenger, R.N. Louie, Appl. Phys. Lett. 76 (2000) 930–932.
[24] C. Su, L. Huang, K. Kjoller, Ultramicroscopy 100 (2004) 233–239.
[25] S. Timoshenko, J. Goodier, Theory of Elasticity, second ed., McGraw–Hill Book Company, New York, 1951.
[26] L.M. Dorogin, S. Vlassov, B. Polyakov, M. Antsov, R. Lõhmus, I. Kink, A.E. Romanov, Phys. Status Solidi B 250 (2013) 305–317.
[27] A.I. Mikhailin, A.E. Romanov, Sov. Phys. Solid State 28 (2) (1986) 337–338.
[28] D.R. Smith, F.R. Fickett, J. Res. Natl. Inst. Stand. Technol. 100 (1995) 119–171.
[29] S. Ogata, J. Li, N. Hirosaki, Y. Shibutani, S. Yip, Phys. Rev. B 70 (2004) 104104.
[30] C. Lu, Phys. Lett. A372 (2008) 6113–6115.
[31] A.H. Barber, Compos. Sci. Technol. 65 (2005) 2380–2384.
[32] S. Cuenot, C. Fretigny, S. Demoustier–Champagne, B. Nysten, Phys. Rev. B 69 (2004) 165410.
[33] J. Reyes–Gasga, J.L. Elechiguerra, C. Liu, A. Camacho–Bragado, J.M. Montejano–Carrizales, M. Jose Yacaman, J. Cryst. Growth 286 (2006) 162–172.
[34] Y. Gao, L. Song, P. Jiang, L.F. Liu, X.Q. Yan, Z.P. Zhou, D.F. Liu, J.X. Wang, H.J. Yuan, Z.X. Zhang, X.W. Zhao, X.Y. Dou, W.Y. Zhou, G. Wang, S.S. Xie, H.Y. Chen, J.Q. Li, J. Cryst. Growth 276 (2005) 606–612.
[35] Y. Ding, P. Zhang, Z. Long, Y. Jiang, J. Yin, F. Xu, Y. Zuo, J. Alloys Compd. 474 (2009) 223–225.
[36] E.W. Weisstein, Area Moment of Inertia, from MathWorld, A Wolfram Web Resource. http://mathworld.wolfram.com/AreaMomentofInertia.html.